Bacterial cellulose–SiO2@TiO2 organic–inorganic hybrid membranes with self-cleaning properties

A. Monteiro, R. Domeneguetti, M. Wong Chi Man, H. Barud, E. Teixeira-Neto, S. Ribeiro

Bacterial Cellulose-SiO_2@TiO_2 Organic-Inorganic Hybrid membranes with Self-Cleaning Properties

A. S. Monteiro[1], R. R. Domeneguetti[1], M. Wong Chi Man[2], H. S. Barud[3], E. Teixeira-Neto[4] and S. J. L. Ribeiro[1]

1 Institute of Chemistry – São Paulo State University – UNESP, Araraquara, São Paulo 14800-970, Brazil

2 Institut Charles Gerhardt Montpellier, UMR5253 CNRS-UM2-ENSCM-UM1, 34296 Montpellier, France

3 University of Araraquara – UNIARA, Araraquara, São Paulo 14801-320, Brazil

4 Brazilian Nanotechnology National Laboratory (LNNano), Brazilian Center for Research in Energy and Materials (CNPEM), Campinas, São Paulo, Brazil

*Corresponding author. Tel.: +551633019631; Email address: sidney@iq.unesp.br (Sidney J. L. Ribeiro)

Highlights

- Development of novel functional bacterial cellulose membranes with self-cleaning properties.
- Decomposition of methyl violet 2B dye in solution through a photocatalytic process.
- High resistance to washing (self-cleaning performance).
- Original features of the membranes (color and texture) maintained.
- Significant reduction of cleaning actions, allowing a reduction in costs and greater durability of the bacterial cellulose membrane.
- Environmentally friendly cellulose membrane.

Abstract
This work reports the preparation of bacterial cellulose (BC) membrane with self-cleaning properties. SiO_2@TiO_2 (anatase) spherical nanocomposites (around 50 nm in diameter) were prepared by a sol-gel process and were successfully immobilized into the BC membrane, in wet and dry states, by post-grafting method, following two different methodologies: dip-coating and spin-coating. Characterization techniques included Raman scattering, Energy-Dispersive X-ray Spectroscopy (EDS), thermogravimetric analyses (TGA), and Scanning Electron Microscopy (SEM). The photocatalytic activity was higher in BC membrane in the wet state, presenting a good self-cleaning performance (fast methyl violet 2B dye decomposition in 30 minutes). The functional BC membranes with self-cleaning properties also presented a high resistance to washing, high chemical stability, and the original features (color and texture) were maintained.

Keywords Functional Bacterial Cellulose Membrane; SiO_2@TiO_2 (anatase) nanocomposites; Photocatalytic Activity; Self-Cleaning Properties; Dip-coating; Spin-coating.

1 Introduction

Cellulose is the most abundant biopolymer on earth and exist in two native forms: the complex cellulose, including most of the cellulose present in nature, and pure cellulose including cellulose produced in their natural state, such as cotton and Bacterial cellulose (BC) [1, 2]. BC is obtained through the biosynthesis induced by *Glucanacetobacter xylinus* which are gram-glycerol and other organic substrates into cellulose in a few days [3, 4]. BC unique structure shows entangled thin nanofibers with a diameter of 20-100 nm, with a large surface area per unit [5]. This feature, in addition to the hydrophilic nature of BC, results in high water absorption capacity, leading to increased moisture content [6-8]. These properties, combined with the distinct physical and mechanical properties of the molecule, including insolubility, biocompatibility, high crystallinity, high swelling, rapid biodegradability, tensile strength, elasticity, durability, nontoxic and nonallergenic features [8-10], make BC ideal for the design of several functional subtrates with high added value. Indeed, with the presence of a large number of hydroxyl groups within their structure, these building blocks, represent a unique platform for surface modification with functional molecules [11]. This is a remarkably versatile biomaterial used in wide variety of domains, such as papermaking, optics, electronics, acoustics, and biomedical devices and still with application such as complementary nutrition, artificial temporary skin for wounds and burns, dental aid, artificial blood vessels, composite reinforcement, electronic paper, light emitting diodes and fuel cell membranes [11-15]. Although it is a reality for medical applications, BC has promising potentials for other applications. The design of materials with functional properties has been a major target, motivated by the consumers and markets demand for high-performance and innovative technologies [16]. Much work has been conducted in development of subtrates with self-cleaning properties [11, 15, 17-22]. Substrates with self-cleaning technology, have the capacity to degrade dirt, odors, and microorganisms through a photocatalytic process, allowing a reduction of cleaning actions and increase of the durability of the substrates [18]. Titanium dioxide (TiO_2) is the most used among the photocatalysts based on benefit-cost ratio, as well as its electronic suitability [12]. The anatase phase displays a higher photoactivity than rutile and brookite [22, 23, 35]. The rutile phase is thermodynamically stable, and the metastable anatase phase (generally formed at low temperature, e.g., by sol-gel processing) [25], transforms to rutile by heating or even by mechanical grinding [22]. The anatase-to-rutilo phase transformation is markedly influenced by the nature and

the amount of cation [19, 20, 22, 26] and anion impurities [27] present in the system, grain size [22], and preparation conditions such as reaction atmosphere. Alternatively, TiO_2 can be grown at the surface of thermally stable, low cost and high-surface-area core materials [22, 28, 29] such as silica. SiO_2 is one of the best core materials for preparing the core@shell nanoparticles due to its rich and well-know surface chemistry and adsorption capacity [30], easy and controllable preparation by the Stöber method [31], optical transparency in the wavelength region where TiO_2 absorbs, low cost and high thermal and mechanical stability [32]. Furthermore, the SiO_2-TiO_2 heterogeneous system often exhibits better photocatalytic activity than TiO_2 alone [33] due to the improved stability of silica-supported anatase and presence of oxygen vacancies in the supported titania [32] as well as due to the improved adsorption of the reactants near the active centers [34].

In the present work, the BC membrane with self-cleaning properties was developed by the immobilization of SiO_2@TiO_2 nanocomposite in the BC membranes. Never-dried and dried BC membranes were used. Dip-coating and spin-coating processes could be compared. The morphology and chemical composition of the SiO_2@TiO_2 nanocomposite and functional BC membranes were characterized. The photocatalytic activity was also evaluated as well as leaching of the nanocomposite.

2 Experimental

2.1 Material and Reagents

Titanium tetraisopropoxide, TIP (97%), nitric acid (70%), acetic acid (90%), aqueous hexadecyltrimethylammonium chloride solution, CTAC (25 wt %) and ammonium nitrate (analytical grade), were purchased from Sigma-Aldrich, agar and tetraethylorthosilicate, TEOS (≥99%) were from Merck, yeast extract was from Kasvi, peptone G was from Acumedia, d-glucose anhydrous (analytical grade), dissodium hydrogen phosphate (analytical grade), citric acid (analytical grade) magnesium sulphate heptahydrate (analytical grade), phosphate monopotassium (analytical grade), sodium hydroxide (analytical grade), Triethanolamine, TEA (≥99,5%) and hydrochloric acid (37%, analytical grade), were supplied by Synth. Ethanol (99,8%, analytical grade) was purchased from Lac. Ultrapure water (Milipore, specific resistivity: 18 MΩ cm) was used throughout the experiments.

2.2 Preparation of SiO_2@TiO_2 nanocomposites

The preparation of SiO_2@TiO_2 nanocomposites were performed following procedures adapted from literature [35] and is described below.

2.3 Preparation of TiO_2 sols

For the preparation of TiO_2 sol, 5 mL titanium tetraisopropoxide (TIP) (3.52 mmol) was added dropwise into 100 mL acidic water (55.5 mmol) containing 1 mL nitric acid (15.7 mmol) and 10 ml acetic acid (0.181 mol) under vigorous stirring (800 rpm). The mixture was stirred for 16 h at 60 °C (pH = 1-2). The resulting sample will be denoted as TiO_2.

2.4 Preparation of SiO_2 nanoparticles

SiO_2 nanoparticles were synthesized by hydrolysis/condensation between tetraethylorthosilicate (TEOS), triethanolamine (TEA), and hexadecyltrimethylammonium chloride (CTAC) according to literature [36]. A stock solution containing 64.0 mL of water (3.55 mol), 10.5 mL of ethanol (0.179 mol) and 10.4 mL of 25 wt% CTAC solution (7.86 mmol) was stirred (800 rpm) for 10 min at room temperature. To this solution, 4.1 mL of TEA (0.031 mol) were added (pH 11). Afterward,

60 mL of this solution were heated to 60 °C and then 4.35 mL of TEOS (19.5 mmol) was added under vigorous stirring (800 rpm). The reaction mixture was stirred at 60 °C for 2 h and then cooled to room temperature. Finally, 150 mL of ethanol (2.57 mol) was added and the resulting SiO_2 nanoparticles were isolated by centrifugation followed by template extration (CTAC). Template removal was performed by refluxing the nanosilicas twice in 150 mL of an ethanolic solution of ammonium nitrate (0.25 M) for 1 h and twice in 150 mL of an ethanolic solution of hydrochloric acid (0.14 M) for 1 h. Afterward the SiO_2 nanoparticles were separated by centrifugation, washed/centrifuged with ethanol twice, and finally was dried at 80 °C for 12 h. The final molar composition of the reagents in the reaction mixtures was TEOS : CTAC : TEA: water : ethanol = 1 : 0.27 : 1 : 137 : 6.2. A molar ratio of TEOS:TEA of 1:1 was chosen to minimize the particle size [37, 38]. The resulting sample will be named as SiO_2.

2.5 SiO_2@TiO_2 nanocomposites

In tota, 1 g of as-prepared SiO_2 nanoparticles was added to TiO_2 sol and dispersed in an ultrasonic bath for 15 min. The SiO_2-TiO_2 mixture was kept for 12 h leadint to TiO_2-supported SiO_2 spherical nanocomposites (pH = 3-5). The resulting sample is denoted as SiO_2@TiO_2. The final molar composition of the components was SiO_2:TIP:water:nitric acid:acetic acid = 1:0.21:3.3:1:10. The solid was separated by centrifugation and dried at 80 °C for 12 h, for subsequent physicochemical characterization.

2.6 Preparation of the bacterial cellulose (BC) membranes

BC membranes were prepared following procedures adapted from literature [37]. The strain used was *Gluconacetobacter xylinus* (ATCC23760) supplied by André Tobello Foundation, Campinas-SP, Brazil. An aliquot of the bacterium *Gluconacetobacter xylinus* (ATCC23760) suspension was replicated to a sterile solid medium plate HS (Hestrim-Schramm) containing 12 g of glucose (0.067 mol), 3 g of yeast extract, 3 g of peptone G, 1.62 g of dissodium hydrogen phosphate (0.011 mol), 0.69 g of citric acid (3,59 mmol), 15 g of agar and 585 mL of milipore water (32.5 mol). After growth time, the microorganism was innoculated into sterile liquid culture medium consisting of 50 g of glucose (0.277 mol), 4 g of yeast extract, 0.73 g of magnesium sulphate heptahydrate(2.96 mmol), 2 g of monopotassium phosphate (0.015 mol), 20 mL of ethanol (0.342 mol) and 980 mL of milipore water (54.4 mol) and kept at 28 °C for 72 h with air circulation. Membranes so produced were subjected to water exchange 5 times per day for 3 days; heated in water at 80 °C for 50 min; immersed in 100 mL of an ethanolic solution of NaOH (0.1 mol L^{-1}) at 80 °C during 50 min and washed again with water until pH 7.0. The resulting non-dried sampleis noted as BCW. BCW was dried at room temperature for 24 h. The resulting dried sampleis denoted BCD.

2.7 Immobilization of SiO_2@TiO_2 nanocomposites on the BC membrane

In total 15 cm (length) x 5 cm (width) rectangular pieces (average weight = 0.3 g) of pristine BCW and BCD membranes were used. SiO_2@TiO_2 nanocomposites were deposited either by dip-coating or spin-coating (scheme 1). In dip-coating, BC membranes was dipped into the SiO_2@TiO_2 nanocomposite suspension during 5 min and then dried at room temperature for 24 h. The resulting samples are BCW-SiO_2@TiO_2-Dip and BCD-SiO_2@TiO_2-Dip, for the never-dried and dried BC membrane,s respectivelly. In spin-coating, 5 mL of the SiO_2@TiO_2 nanocomposite solution were deposited on the center of the BC membrane; subsequently, the BC membrane was rotated at 3000 rpm during 30 s, and then dried at room temperature during 24 h. The resulting samples are denoted, BCW-SiO_2@TiO_2-Spin and BCD-SiO_2@TiO_2-Spin, for the never-

dried and dried BC membranes, respectivelly. After functionalization, all membranes, were subjected to a hydrothermal treatment, at 150 °C for 4 h and dried again at room temperature during 24 h.

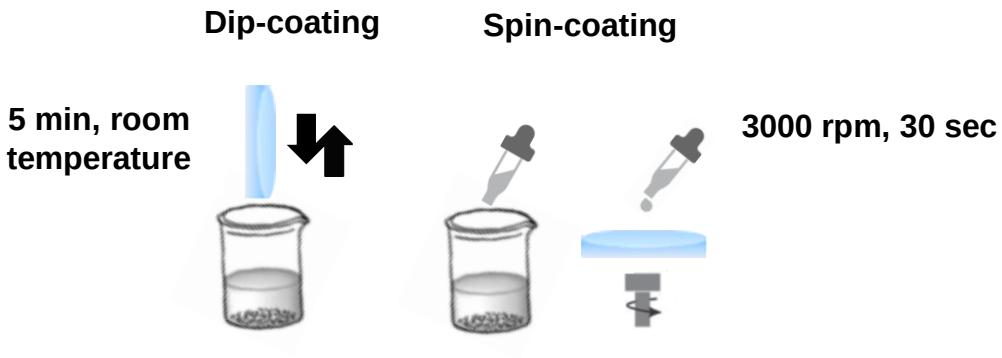

Scheme 1 Schematic representation of the immobilization process by dip-coating and spin-coating, of SiO_2@TiO_2 nanocomposite on bacterial cellulose membrane

2.8 Characterization

The interaction between the SiO_2 and TiO_2 component was analyzed by attenuated total reflectance Fourier transform infrared (FTIR-ATR) spectroscopy. The FTIR-ATR spectra were obtained with a Bruker Vertex 70 spectrophotometer in the range of 400–4000 cm^{-1}, with 4 cm^{-1} resolution and 16 scans. Raman spectra were obtained with a Labram HR 800, Horiba Jobin Yvon Raman Spectrometer, equipped with He–Ne 632.81-nm laser and CCD (DU420A-OE-325 model) detector. The spectra were acquired with a laser power of 150 mV using an integration time of 300 s and 20 runs per measurement. The crystal phase of the SiO_2@TiO_2 nanocomposite solid powder extracted was studied by Xray diffraction (XRD). The measurements were performed at room temperature with a Siemens D5000 Diffrac Plus XRD commander diffractometer, using Cu Kα radiation (λ = 1.5406 Å) and Bragg–Brentano θ/2θ configuration. The morphology and size of SiO2, TiO_2, the SiO_2@TiO_2 nanocomposite and the BC membrane, and functional BC membranes were investigated by scanning electron microscopy (SEM) and scanning transmission electron microscopy (STEM). SEM micrographs were performed using a high-resolution environmental scanning electron microscope (JEOL JSM7500-F model). Samples SiO_2 and SiO_2@TiO_2 were analyzed in powder, while sample TiO_2 was analyzed in solution (an aliquot was deposited on carbon tape attached to the support and dried under vacuum for 8 h) and covered with a 1-nm-thick carbon layer. The average particle size and standard deviations of silica nanoparticles were calculated from the diameters of more than 50 particles randomly selected from SEM micrographs and using the ImageJ software. The STEM images were collected at the Brazilian Nanotechnology National Laboratory (LNNano), Brazilian Center for Research in Energy and Materials (CNPEM), Campinas, Brazil, in a JEOL-JEM 2100 F microscope operated at 80 kV. The TiO_2 and SiO_2 contents were obtained by X-ray fluorescence analysis (XRFA) at the Department of Chemistry, University of São Paulo (USP, São Carlos, Brazil), using a benchmark MiniPal4 (PANalytical) spectrometer in energydispersive mode. The semiquantitative determination of TiO_2 and SiO_2 was performed using the standardless analysis package Omnian (PANalytical). All the measurements were acquired after a total measurement time of 840 s and were done in triplicate. Thermogravimetric analyses (TGA) of the BC membrane and functional BC membranes were carried out on a SDT 2960 from TA-

Instruments. Samples were heated from 50 to 700 °C under an oxygen atmosphere, 200 mL min^{-1}, at a heating rate of 5 °C min^{-1}.

2.9 Dye photodecomposition

The self-cleaning properties of functional cellulose membranes, CB@SiO_2@TiO_2 were evaluated by observing the decomposition of adsorbed methyl violet 2B (MV). The absorbance peak of methyl violet 2B (MV) dye in the visible region (450–700 nm) was measured after each dosage of irradiation of UV light (5–30 min). Cellulose membranes were dipped in aqueous solution of MV dye (0.1%), for 5 min and then dried for 1 h at room temperature. Afterward, 5 cm × 5 cm of the cellulose membrane was coated with aluminum foil and then placed under UV radiation (10 cm × 5 cm). The sample–lamp distance was 7 cm. A solar light simulator system, based on a Xe 150-W lamp, the range of emission wavelength between 290 and 400 nm (UVA and UVB) (16S-150W model, Solar Light, Inc., Philadelphia, USA) and a UV-Vis spectrometer (Carry 5000 model) was used.

2.10 Resistance to washing

In order to evaluate the stability of the SiO_2@TiO_2 containing BC membranes, the samples BCW–SiO_2@TiO_2–dip and BCW–SiO_2@TiO_2–spin were placed in water in an ultrasonic bath at room temperature for 20 min and then dried at room temperature for 24 h. Subsequently, the self-cleaning properties were evaluated.

3 Results and discussion

3.1 SiO_2@TiO_2

Figure 1 shows SEM micrographs of the samples of SiO_2 as spherical nanoparticles with an average diameter of (51 ± 15) nm (Fig. 1a), TiO_2 as a film consisting of fine grains (Fig. 1b), and SiO_2@TiO_2 (Fig. 1c).

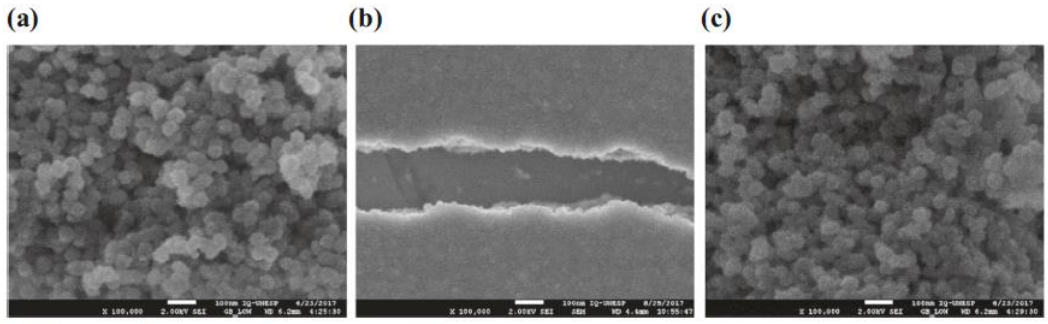

Fig. 1 SEM micrographs of **a** SiO_2, **b** TiO_2, and **c** SiO_2@TiO_2

The SEM (Fig. 1c) and STEM (Fig. 2) micrographs of SiO_2@TiO_2 show spherical nanoparticles with an average diameter of (52 ± 10) nm. Xray elemental maps from STEM (Fig. 2) reveal the presence of Ti in addition to the Si and O (from SiO_2), in SiO_2@-TiO_2. A heterogeneous Ti mapping on the SiO_2 nanoparticles is observed, suggesting a thin layer of the TiO_2 on the SiO_2 nanoparticles (dark sides with slight red spots) and between these, where the Ti concentration is higher (intense red parts).

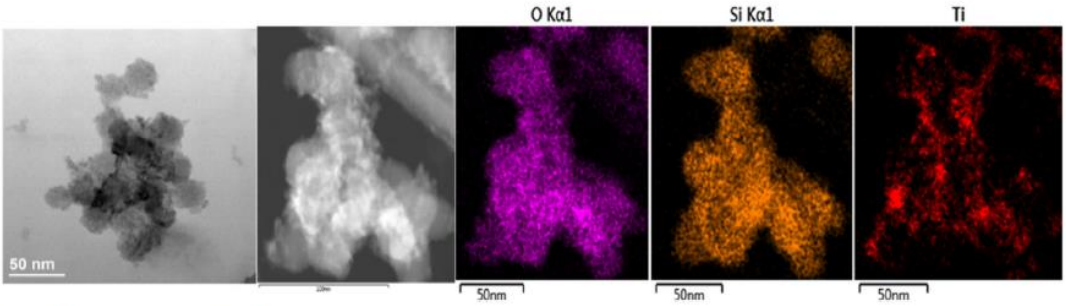

Fig. 2 STEM micrographs of SiO_2@TiO_2 nanocomposites and the corresponding X-ray maps

FTIR-ATR spectra of the samples of SiO_2 (Fig. 3a) and SiO_2@TiO_2 nanocomposites (Fig. 3b) are shown in Fig. 3. Both spectra show a broad band centered at 3460 cm^{-1} and attributed to O–H stretching vibrations of surface silanols and the remaining physisorbed water; a band at 1639 cm^{-1} related to the bending vibrations of adsorbed water; characteristic bands of silica: a strong intensity band centered at 1068 cm^{-1} with a shoulder at 1239 cm^{-1} assigned to asymmetric Si–O–Si stretching vibrations; and a band at 800 cm^{-1} assigned to symmetric Si–O–Si stretching [5, 39]. The interaction between TiO_2 and SiO_2 in the SiO_2@TiO_2 nanocomposite (Fig. 3b) is shown by the band at 946 cm^{-1} assigned to the symmetric Ti–O–Si stretching band, confirming that the SiO_2 reacted with TiO_2 to form the Ti–O–Si structure [35]. In the FTIR-ATR spectrum of SiO_2@TiO_2 (Fig. 3b), two other bands are observed: at 1404 cm^{-1}, corresponding to the Ti–O–Ti stretching vibration [40] and at 1703 cm^{-1} assigned to C = O vibration of the carboxylic group (–COOH) of acetic acid, not involved in Ti chelation [41]. According to literature [35], the formation mechanism of the SiO_2@TiO_2 nanocomposite is considered by electrostatic deposition. The isoelectric point of TiO_2 is 5.5 and that of the SiO_2 particles ranged from 1.8 to 2.7 [42, 43]. As the pH value was 3–5, the TiO_2 would have a positive surface charge density and the SiO_2 nanoparticles would have a negative surface charge density. Thus, TiO_2 could be deposited on the surface of the SiO_2 nanoparticles driven by the electrostatic attraction between TiO_2 and SiO_2. SiO_2 (95.6 ± 0.2) and TiO_2 (4.4 ± 0.3) contents of the SiO_2@TiO_2 nanocomposites were estimated by X-ray fluorescence analysis (XRFA) (Table 1).

Table 1 SiO_2 and TiO_2 relative contents of the SiO_2@TiO_2 nanocomposites estimated by XRFA

Sample	%SiO_2 (wt/wt)	%TiO_2 (wt/wt)
SiO_2@TiO_2	66.2 ± 0.2	3.0 ± 0.3
Normalized to 100% SiO_2@TiO_2	95.6 ± 0.2	4.4 ± 0.3

Figure 4 shows the XRD patterns of the SiO_2@TiO_2 nanocomposite. Anatase peaks at 25.3°, 38.1°, and 48.2° and no traces of brookite or rutile were observed, indicating that single-phase anatase nanocrystallites were formed. The phase anatase TiO_2 has the highest photoactivity among different crystal phases of TiO_2 [22, 23, 35].

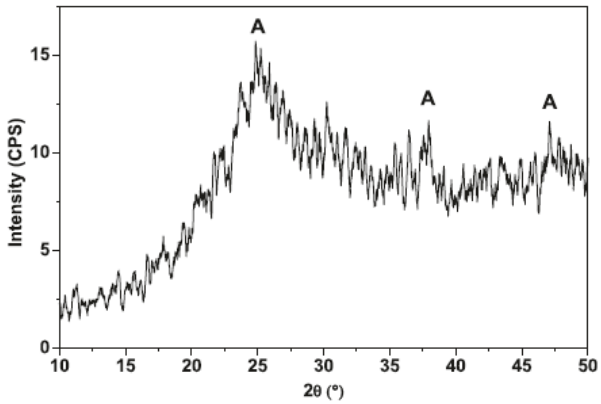

Fig. 4 Wide-angle X-ray diffractograms of powder extracted from colloid SiO_2@TiO_2 nanocomposites (A anatase)

3.2 Photocatalytic BC–SiO_2@TiO_2 membranes

SEM micrographs and EDS spectra of the BC membrane (a) and BC–SiO_2@TiO_2 membranes (b–e) are illustrated in Fig. 5. SEM micrographs of the BC membrane exhibit smooth longitudinal fiber-like structures (Fig. 5a), while those of BC–SiO_2@TiO_2 membranes reveal BC fibers coated with particles, imparting surface roughness in the fibers. In the case of BCW–SiO_2@TiO_2–dip (Fig. 5c) and BCW–SiO_2@TiO_2–spin (Fig. 5e), the surface of the fibers is coated with particles with the same morphology and average particle size (52 ± 10) nm as those of SiO_2@TiO_2 (Fig. 1c). In BCD–SiO_2@TiO_2–dip (Fig. 5b), the BC fibers are fully covered with a film of an agglomerate of these nanoparticles. In the case of BCD–SiO_2@TiO_2–spin (Fig. 5d), one can see thick layers upon which electron beams have been cracked. Beyond these layers, the BC fibers are fully covered with these particles (Fig. 1b). The EDS spectra (Fig. 5) confirm the existence of Si and Ti in the functional BC membranes, indicating the successful grafting of the SiO_2@TiO_2 nanocomposite in the BC membrane.

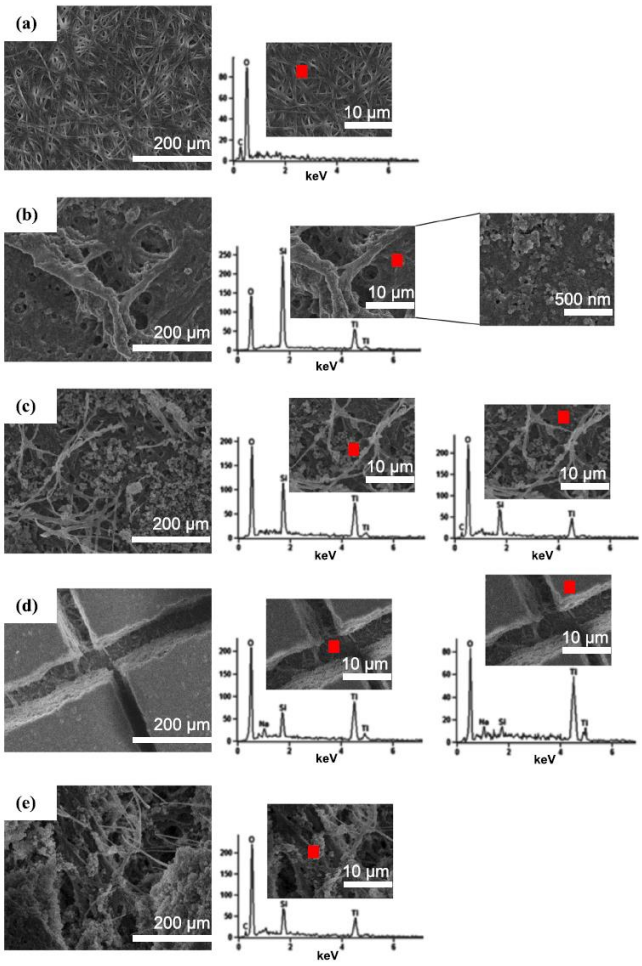

Fig. 5 SEM micrographs and EDS spectra of a) BC, b) BCD–SiO_2@TiO_2–dip, c) BCW–SiO_2@TiO_2–dip, d) BCD–SiO_2@TiO_2–spin, and e)BCW–SiO_2@TiO_2–spin.

Raman spectra of functional BC membranes (Fig. 6) show characteristic bands of anatase at 148 cm^{-1} (Eg), 396 cm^{-1} (B1g), 513 cm^{-1} (A1g/B1g), and 635 cm^{-1} (Eg) [12, 39]. Therefore, anatase crystalline phase remains after immobilization of the SiO_2@TiO_2 nanocomposite in the BC membrane.

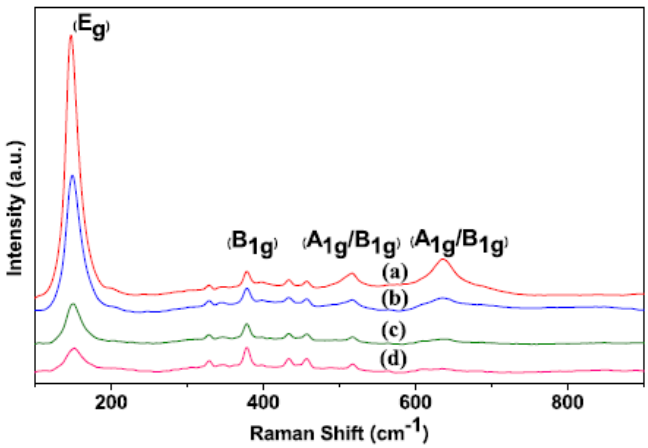

Fig. 6 Raman spectra of **a** BCW–SiO_2@TiO_2–spin (red line), **b** BCD–SiO_2@TiO_2–spin (blue line), **c** BCW–SiO_2@TiO_2–dip (green line), and **d** BCD–SiO_2@TiO_2–dip (pink line)

TGA curves of the BC membrane (a) and functional BC membranes (b–e) are shown in Fig. 7. Two significant weight losses are observed from ambient temperature to 150 °C and from 150 to 500 °C. The first weight loss is due to membrane dehydration. Physically adsorbed and hydrogen-bonded linked water molecules are removed at this first stage. The second weight loss is associated to the decomposition of the CB membrane [5, 40]. From 500 °C, a variable residue is observed, according to the process employed in the immobilization of the SiO_2@TiO_2. The residue loading increases in the order BCD–SiO_2@TiO_2–dip < BCD–SiO_2@TiO_2–spin < BCW–SiO_2@TiO_2–dip <BCW–SiO_2@TiO_2–spin, suggesting a higher immobilization efficiency of the SiO2@TiO2 nanocomposite in the BC membrane in the never-dried state.

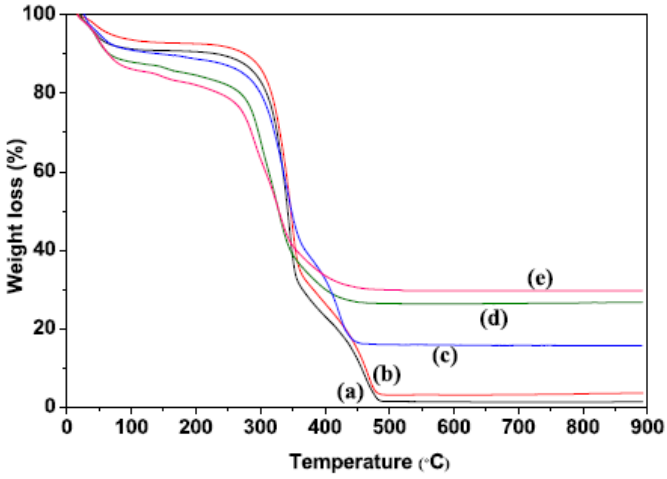

Fig. 7 TGA curves of the samples: **a** BC, **b** BCD–SiO_2@TiO_2–dip, **c** BCD–SiO_2@TiO_2–spin, **d** BCW–SiO_2@TiO_2–dip, and **e** BCW–SiO_2@TiO_2–spin

The self-cleaning properties of membranes were evaluated by measuring the absorption spectra of MV dye in the visible region (450–700 nm) after each UV light dosage (5–30 min) (Fig. 8).

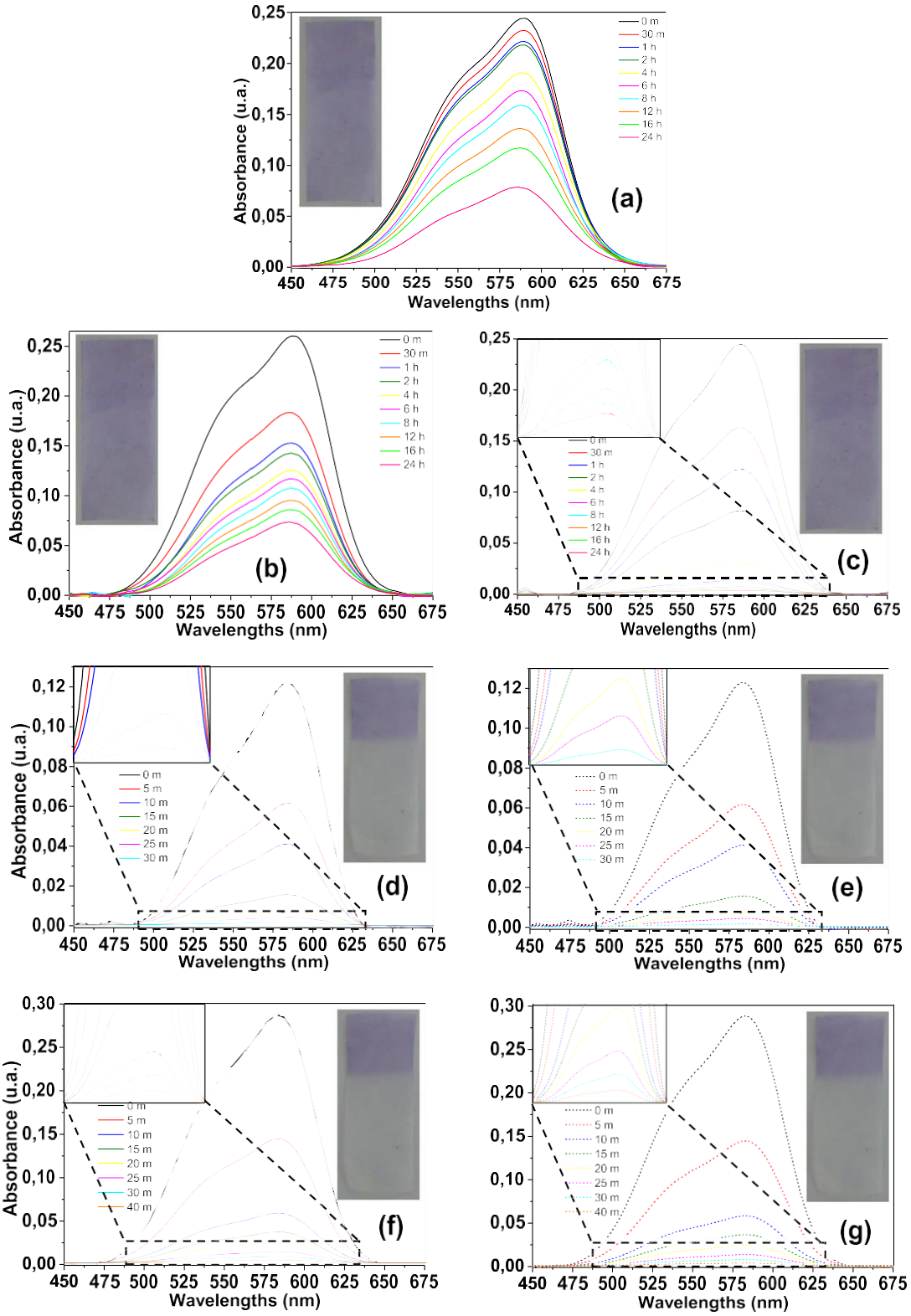

Fig. 8 Electronic absorption spectra of the samples: a pristine BC, b BCD–SiO_2@TiO_2–dip, c BCD–SiO_2@TiO_2–spin, d BCW–SiO_2@TiO_2–dip, e BCW–SiO_2@TiO_2–dip (after washing fastness), f BCW–SiO_2@TiO_2–spin, and g BCW–SiO_2@TiO_2–spin (after washing fastness), with the respective times of UV light irradiation and photograph of the respective samples after irradiation

The MV characteristic band decreases in intensity as a function of the irradiation time. These samples with best efficiency of self-cleaning properties, exhibited a higher loading residue (Fig. 7) and also present good resistance to washing (Fig. 8d vs. 8e and Fig. 8f vs. 8g), as evidenced by the constant performance of self-cleaning properties. The enhanced photocatalytic activity of the functional bacterial BC membrane might be attributed to the unique physicochemical properties of the SiO_2@TiO_2 nanocomposite which result from the strong interaction of the TiO_2 film and SiO_2 nanoparticles, such as the increased specific surface area of the SiO_2@TiO_2 nanocomposite [35, 43] and the enhanced surface acidity of the nanocomposites [35, 44]. The increase in the specific surface area facilitates more effective adsorption sites which might promote the photocatalytic activity by increasing the concentration of contaminants and reaction intermediates near the TiO_2 [35]. Additionally, mixed metal oxides often generate additional surface acidity over their individual members because of an increase in the polarizability of the hydroxide groups present in the mixed oxide [35]. In the SiO_2@TiO_2 nanocomposite, a complex oxide may form at the interface due to the existence of Ti–O–Si vibration in the FTIR spectrum (Fig. 3). These bonds enhance surface acidity of the TiO_2@SiO_2 nanocomposites and in turn improve the photocatalytic activity of the BC–SiO_2@TiO_2 membrane fabricated in this study [35].

4 Conclusion

BC membranes displaying self-cleaning properties have been prepared by incorporation of SiO_2@TiO_2 composites in BC. TGA analyses demonstrate a higher loading for never-dried BC membranes possibly due to a better diffusion of the composite into the BC during the process. This higher loading may correlate with the greater efficiency of the latter materials synthesized in the wet state compared to the other materials to degrade MV in much shorter time. The functional BC membranes also presented a good resistance to washing with high chemical stability and the color and texture of the original features were maintained. The good properties acquired in this versatile biomaterial open the way to obtain functional BC which will find application in several areas.

Acknowledgements This work has been financially supported by Fundação de Amparo à pesquisa do estado de São Paulo (FAPESP), through project 2015/12908-2. ASM is thankful to FAPESP for a grant. The authors thank André Tobello Foundation for effering the strain Gluconacetobacter xylinum (ATCC23760) LNNano-CNPEM (Campinas, Brazil) for the use of the JEOL-JEM 2100 F STEM microscope and Dr. Sajjad Ullah for help in XRFA measurements.

eferences

[1] Pecorano E, Manzani D, Messadeq Y, Ribeiro S J L (2008) In: Belgacem M N, Gandini A (ed) Monomers, Polymers and Composites from Renewable Resources, 1st edn. Elsevier Science

[2] Jozala A F, de Lencastre-Novales L C, Lopes A M, de Carvalho Santos-Ebinuma V, Mazzola P G, Pessoa-Jr A, Grotto D, Gerenutti M, Chaud M V (2016) Appl Microbiol Biotechnol 100:2063

[3] Barud H S, Caiut J M A, Dexpert-Ghys J, Messaddeq Y, Ribeiro S J L (2012) Composites: Part A 43:973

[4] Maeda H, Nakajima M, Hagiwara T, Sawaguchi T, Yano S (2006) J Mater Sci 41:5646

[5] Barud H S, Assunção R M N, Martines M A U, Dexpert-Ghys J, Marques R F C, Messaddeq Y, Ribeiro S J L (2008) J Sol-Gel Sci Technol 46:363

[6] Barud H S, Barrios C, Regiani T, Marques R F C, Verelst M, Dexpert-Ghyo J, Messaddeq Y, Ribeiro S J L (2008) Mat Sci Eng C 28:515

[7] Nishi Y, Uryu M, Yamanaka S, Watanabe K, Kitamura N, Iguchi M, Mitsuhashi S (1990) Mater Sci 25:2997

[8] Legnani C, Legnani C, Vilani C, Calil V L, Barud H S, Quirino W G, Achete C A, Ribeiro S J L, Cremosa M (2008) Thin Sol Films 517:1016

[9] Yano Y, Sugiyama J, Nakagaito A N, Nogi M, Matsuura T, Hikita M, Handa K (2005) Adv Mater 17:153

[10] Barud H S, Souza J L, Santos D B, Crespi M S, Ribeiro C A J, Messaddeq Y, Ribeiro S J L (2011) Carbohydr Polym 83: 1279

[11] Khalid A, Ullah H, Ul-Islam M, Khan R, Khan S, Ahmad F, Khan T, Wahid F (2017) RSC Adv 7:47662

[12] Ullah S, Ferreira-Neto E P, Pasa A A, Alcântara C C J, Acuña J J S, Bilmes S A, Ricci M L M, Landers R, Fermino T Z, Rodrigues-Filho U P (2015) Appl Catal B – environ 179:333

[13] Pinto E R P, Barud H S, Silva R R, Palmieri M Polito W L, Calil V L, Cremosa M, Ribeiro S J L, Messaddeq Y (2015) J Mater Chem C 3:11581

[14] Fujishima A, Zhang X, Tryk D (2008) Surf Sci Rep 63:515

[15] Augustynski J (1993) Electrochim Acta 38:43

[16] Mandzy N, Grulke E, Druffel T, Powder Technol 160:121

[17] Hanaor D A H, Assadi M H N, Li S, Yu A B, Sorrell C C (2012) Comput Mech 50:185

[18] Raj K, Viswanathan B (2009) Indian J Chem 48:1378

[19] Hirano M, Joji T, Inagaki M, Wata H (2004) J Am Ceram Soc 87:35

[20] Hirano M, Nakahara C, Ota K, Tainaike O, Inagaki M (2003) J solid State Chem 170:39

[21] Herrmann J (1999) Catal Today 53:115

[22] Hirano M, Ota K, Iwata H (2004) Chem Mater 16:3725

[23] Banerjee S, Gopal J, Muraleedharan P, Tyagi A, Raj B (2006) Curr Sci 90:1383

[24] Diebold U (2003) Surf Sci Rep 48:53

[25] Barringer E A, Bowen H K (1982) J Am Ceram Soc 65:199

[26] Hirano M, Nakahara C, Ota K, Inagaki M (2002) J Am Ceram Soc 85:1333

[27] Ding X Z, Liu X H (1996) J Mater Sci Lett 15:1789

[28] Son S, Hwang S H, Kim C, Yun J Y, Jang J (2013) ACS Appl Mater Interfaces 5:4815

[29] Hanprasopwattana A, Srinivasan S, Sault A G, Datye A K (1997) Catal Lett 45:165

[30] Iler R (1978) The Chemistry of Silica Wiley-Interscience, New York

[31] Fink A, Stöber W, Bohnn E (1968) J Colloid Interface Sci 26:62

[32] Periyat P, Baiju K, Mukundan P, Pillai P, Warrier K G K (2008) Appl Catal A Gen 349:13

[33] Cheng P, Zheng M, Jin Y, Huang Q, Gu M (2003) Matter Lett 57:2989

[34] Friesen D, Morello L, Headley J V, Lanford C H (2000) Photochem Photobiol A Chem 133:213

[35] Qi K, Chen X, Liu Y, Xin J H, Mak C L, Daoud A (2007) J Mater Chem 17:3504

[36] Kobler J, Möller K, Bein T (2008) ACS nano 2:791

[37] Möller K, Kobler J, Bein T (2007) Adv Funct Mater 17:605

[38] Möller K, Kobler J, Bein T (2007) J Mater Chem 17:624

[39] Socrates G (2004) Infrared and Raman Characteristic Group Frequencies: Tables and Charts, John Wiley & Sons Ltd., Chichester, U.K.

[40] Barud H S, Regiani T, Marques RFC, Lustri W R, Messaddeq Y, Ribeiro S J L (2011) J nanomater 2011:10

[41] Juma A O, Acik I O, Mikli V, Mere A, Krunks M (2015) Thin Solid Films 594:287

[42] Larson I, Drummond C J, Chan D Y C, Grieser F (1993) J Am Chem Soc 115:11885

[43] Subramaniam K, Yiacoumi S, Tsouri C (2000) Colloids Surf A 177:133

[44] Papp J, Soled S, Dwight K, Wold A (1994) Chem Mater 6:496